

# Exotic liquid crystalline phases in monolayers of vertically vibrated granular particles

Y. Martínez-Ratón<sup>a</sup> and E. Velasco<sup>b</sup>

<sup>a</sup> *Grupo Interdisciplinar de Sistemas Complejos (GISC), Departamento de Matemáticas, Escuela Politécnica Superior, Universidad Carlos III de Madrid, Avenida de la Universidad 30, E-28911, Leganés, Madrid, Spain*

<sup>b</sup> *Departamento de Física Teórica de la Materia Condensada, Instituto de Física de la Materia Condensada (IFIMAC) and Instituto de Ciencia de Materiales Nicolás Cabrera, Universidad Autónoma de Madrid, E-28049, Madrid, Spain*

Vibrated monolayers of granular particles confined into horizontal cavities form a variety of fluid patterns with orientational order that resemble equilibrium liquid-crystal phases. In some cases one can identify nematic and smectic patterns that can be understood in terms of classical statistical mechanics of hard bodies. Low aspect ratio cylinders project as rectangles and form uniaxial, or 2-atic, and tetratic, or 4-atic, nematic phases. Other polygonal particles may exhibit different liquid-crystal phases, in general  $p$ -atic phases, of higher symmetries. We give a brief summary of theoretical work on rectangles and triangles, and provide some experimental results on vibrated monolayers. In the case of equilateral triangles, the theory predicts an exotic triatic phase, or 6-atic phase, with six-fold symmetry and three equivalent directors. Right-angled triangles exhibit a 4-atic phase with strong octatic (8-atic) correlations. Experiments on cylinders show 4-atic textures and, even more remarkable, geometric frustration caused by confinement excites topological defects, which seem to follow the same topological rules as standard liquid crystals. Some of our findings can be understood with the help of simulations of hard particles subject to thermal equilibrium, although standard Density-Functional Theories fail to account for the correct equilibrium phases in some cases.

## I. INTRODUCTION

Hard particles continue to generate a lot of interest in condensed-matter physics, not only because of the potential technological applications based on their self-assembling properties, but also because the prominent role that entropy plays in their behaviour. Recent advances in the synthesis of particles have provided the possibility to produce particles with a fine control of their size, shape and interactions (see e.g. [1–3]), opening an enormous field of experimental research concerning phase transitions involving positional and orientational degrees of freedom. By suitable treatment these interactions can be chosen to be very close to hard-core interactions. In solution these particles can be considered as quasi-hard particles subject to Brownian motion and theoretical analyses based on the traditional density-functional theories (DFT) for hard bodies are appropriate. The variety of particles shapes and the subtle entropic forces that operate in these systems have been shown to produce new possibilities for the design of self-assembling materials [4–6] and therefore theoretical studies exploring the fundamental ordering mechanisms have been revitalised.

Recently two-dimensional (2D) hard particles have enjoyed a renewed interest in the liquid-crystal community. Their reduced dimensionality leads to peculiar properties of their phase transitions (nonexistence of long-ranged order and defect-mediated phase transitions), but the possibility that these particles stabilise mesogenic (hence fluid) phases with high-order orientational symmetries (‘exotic’ nematic phases) has attracted much attention [7]. Schlacken et al. [8] used the Scaled-Particle Theory (SPT) version of DFT, based on two-particle correlations via the second virial coefficient, to analyse fluids of hard rectangles, and an intermediate tetratic phase, with four-fold symmetry, was predicted to stabilise for relatively low aspect ratios. This is in contrast to the standard uniaxial nematic phase with twofold symmetry in systems of rods with head-tail symmetry. Later, a more complete fluid phase diagram was obtained using the same theory [9], and the effect of three-body correlations was assessed [10] and seen to reinforce tetratic order. Other convex hard particles with polygonal shape have been examined using the same theoretical approach, and phases with triatic, or sixfold, symmetry, were predicted in fluids of particles with isosceles triangular shape close to the equilateral condition [11]. More recently, fluids of hard right-angled triangles (HRT) have been seen to present evidences of strong octatic, or eightfold, orientational correlations, which constitutes a challenge for the standard DFT theories [12].

On the simulation side, orientational order in fluids made of anisotropic hard particles has been studied by many authors. Nematic phases have quasi-long-range order and are obtained from the isotropic through a continuous transition driven by a Kosterlitz-Thouless mechanism [13]. Focussing on hard or quasi-hard particles of convex polygonal shape, phases with tetratic phases were initially studied in squares [14] and then confirmed by several studies [15–17]. Hard rectangles have also been studied but with not so much emphasis on the tetratic phase [18, 19]. Recently fluids of HRT particles have been seen to exhibit peculiar orientational properties [12, 20], with strong indications of quasi-eightfold symmetry. Other particle shapes such as pentagons and hexagons have been analysed

[18]. As expected, the latter form a fluid phase with sixfold symmetry

Lithographic techniques are being applied in the production of particles with specific polygonal shapes [1–3]. These particles behave as Brownian particles when in solution, and can be arranged in monolayers. Also, filamentous virus particles can be engineered to control particle stiffness. Ordering properties of such systems under confinement have been explored and compared with elastic and microscopic theories [21]. These developments open up the possibility to experimentally study the effect of entropy on 2D orientational ordering and, in addition, to provide data against which standard and new theories can be contrasted.

Another field of research in this area has emerged recently. Vertically vibrated monolayers of granular macroscopic particles confined into horizontal cavities have been shown to provide a useful setting to probe 2D fluid ordering. Narayan et al. [22] observed uniaxial nematic and tetratic phases in systems of quasi-2D metallic cylinders (which project horizontally as quasirectangles). Galanis et al. [23, 24] studied uniaxial nematic ordering of metallic needles and concluded that the standard elastic theory of liquid crystals can be used to explain some features of the experimental results, such as emergence of nematic order and the competition with orientation at a surface boundary, in what appears to be a kind of ‘entropic anchoring’ mechanism [25]. Using Monte Carlo (MC) simulation, the equilibrium nematic and tetratic phase behaviour of rectangles has been compared with the behaviour of vibrated monolayers [26], and reasonable overall agreement was found in controlled regions of parameter space. Also, comparison of clustering effects and ordering between the equilibrium and dissipative systems, and also the formation of topological defects, has been made [27, 28]. All these studies point to a rich phenomenology and to subtle entropic effects giving rise to nontrivial symmetries and response to external fields in systems of particles with relatively simple shapes.

A striking effect in systems of regular, or not very nonregular, polygonal shapes, is the occurrence of nematic phases with high symmetries, i.e. higher than the standard uniaxial symmetry found in fluids of rods with head-tail particle symmetry. The tetratic phase formed by hard rectangles of low aspect ratio is the simplest of these phases. In general polygonal-shaped particles can give rise to the so-called  $p$ -atic fluid phases. In these phases the orientational distribution function  $h(\phi)$ , giving the probability that, on average, a particle is oriented along some direction  $\phi$  with respect to some fixed axis, exhibits rotational symmetry by a multiple of  $2\pi/p$ , with  $p = 2, 3, 4, \dots$ . The standard uniaxial nematic would have  $p = 2$ . Hard rectangular particles (including squares) have been shown to stabilise into a tetratic phase, with  $p = 4$ . Recently Anderson et al. [18] have conducted systematic simulations on various types of particles and shown that some regular polygonal particles exhibit  $p$ -atic phases: equilateral triangles (6-atic), squares (4-atic), and hexagons (6-atic). Regular polygons with seven edges or more behave as hard discs in that the isotropic (I) phase crystallises via first a continuous transition to a hexatic fluid and then a first-order transition to a crystal, without liquid-crystal behaviour. However, polygons with fewer than seven edges very easily align with respect to their neighbours and a local liquid-crystalline order is imposed, giving rise to  $p$ -atic phases that transform into the isotropic via a KTHNY mechanism. Regular pentagons are special because of the incompatibility of the corresponding 5-atic symmetry with a regular crystal and no liquid-crystal phase results, with an isotropic phase that directly crystallises into a solid via a first-order phase transition.

However, there are strong indications that systems of particles made of *nonregular* polygonal shapes may form intermediate orientational phases of nontrivial symmetries due to clustering mechanisms [12]. In equilibrium the clustering tendency is driven by entropic forces [29, 30], and additionally dissipation may contribute in vibrated monolayers [27]. By nontrivial symmetry we mean a symmetry which does not arise directly from particle shape. In this work we discuss the case of HRT fluids, which seem to exhibit a 4-atic phase but with very strong 8-atic (or octatic) correlations. This symmetry can only result from the coexistence of several types of particle clusters, including dimers and tetramers. Recent simulation results [12] indicate that the fractions of these clusters are such that the global phase is almost perfectly 8-atic. By contrast, the standard DFT approximation, based on the second and third virial coefficients, is unable to deal with the high-order correlations needed to explain the formation of some of these clusters. This is an unusual situation in the theory of liquid crystals, as the standard DFT approach, originating from Onsager[31], has been very successful to explain the occurrence and symmetries of liquid-crystal phases both in 2D and 3D, at least at the qualitative level. These negative results point to the need for a serious improvement of the theory in its application to 2D fluids of hard convex particles of nonregular polygonal shape.

In this article we describe some of our recent work on the orientational phase behaviour of some 2D hard particles, which covers both theoretical (predictions on phase diagrams based on DFT and MC simulation) and experimental results on monolayers of vibrated granular particles. The conclusions gravitate about three basic points: (i) The standard DFT, based on two-body angular correlations, gives essentially correct predictions as to the equilibrium orientational phases, provided the particles consist of regular or close to regular polygons. (ii) For some non-regular polygonal particles the tendency of particles to cluster into well-identified groups of particles with a definite symmetry may be very strong; in these cases the symmetry of the bulk phase may not be evident from the particle symmetry and the DFT approach may fail dramatically. In particular, symmetries that do not follow directly from particle shape, such as the 8-atic symmetry, may result from particle clustering in the case of HRT. (iii) Vibrated monolayers of particles show many common features with the equilibrium counterparts: bulk ordering and symmetry, response

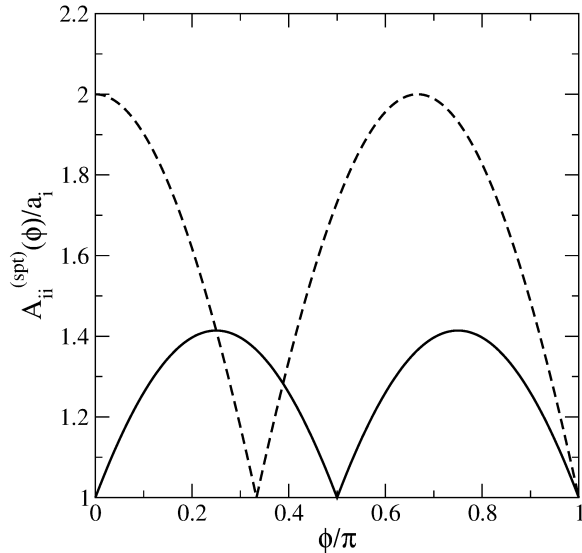


FIG. 1: SPT areas (scaled with particle area) between two hard squares (solid) and two equilateral triangles (dashed).

to external fields and excitation of defects under geometrical frustration. These systems may represent a fruitful approach to study order in 2D fluids of hard particles, complementary to experiments on Brownian particles and to theoretical approaches.

The paper is organised as follows. In Section II we review the SPT version of DFT theory applied to general 2D hard particles, and its extension to incorporate three-body correlations through an orientational-dependent third-virial coefficient. Also, we show some results for the 2-atic and 4-atic phases of hard rectangles (HR), and for the 6-atic phase of triangles (HT) close to equilateral, to make clear the connection between the bulk symmetry and the (microscopic) orientational distribution function. Section III is devoted to the theoretical results on phase diagrams. The fluid phase diagram of one-component HR is discussed, and the strong effect of three-body correlations emphasised, pointing to the importance of clustering in the structure of these systems. Next, the phase behaviour of a fluid of HT particles is shown, as a function of the opening angle and in the framework of the SPT theory. In addition, the fluid of HRT is discussed, with a focus on the evidence from simulation on the existence of strong eight-fold correlations in this system. Both the standard SPT version of DFT, and the extended version with the third virial coefficient, fail to reproduce this symmetry, without the slightest hint of secondary peaks in a completely uniaxial orientational distribution function. We present evidence from simulation for the formation of strong clustering in this fluid, and discuss a model based on a quaternary mixture of particles with shapes given by the clusters coexisting in the configurations observed in the simulations. This model, although not fully consistent, is an extension of SPT theory and provides a mechanism that can explain the presence of such strong 8-atic correlations in the system. In Section IV we present our results on experiments made on vibrated quasimonoayers of metallic particles. Steady-state 4-atic configurations are stabilised in monolayers of cylinders (which behave as hard rectangles), and the imposed circular symmetry of the confining cavity creates topological defects which agree in charge and structure with the predictions of topology and equilibrium statistical mechanics. Other geometries are discussed and the results explained in terms of the breakdown of the continuum hypothesis implicit in the elastic theory of liquid crystals. We end in Section V with some conclusions.

## II. THEORY

In this section we review the standard DFT theory for 2D liquid crystals, as applied to a fluid mixture of hard bodies. The theory is based on an approximate expression for the excess or interaction part of the Helmholtz free-energy,  $\beta\mathcal{F}_{\text{ex}}[\{\rho_i\}]$ , as a functional of the density profile of species  $i$  ( $i$  varying from 1 to the total number of components),  $\rho_i(\mathbf{r}, \hat{\omega})$ , with  $\mathbf{r}$  and  $\hat{\omega}$  the position vector of the centre of mass and the unit vector parallel to the main particle axis of the  $i$ th species, respectively. We restrict our study to orientationally ordered uniform phases of 2D uniaxial particles, i.e. the density profiles,  $\rho_i(\phi)$ , only depend on a single angular coordinate,  $\phi$ , the angle between the main particle axis and one of the fixed Cartesian axis.

One of the most commonly used versions of DFT is SPT [32–37]. This theory successfully describes the phase

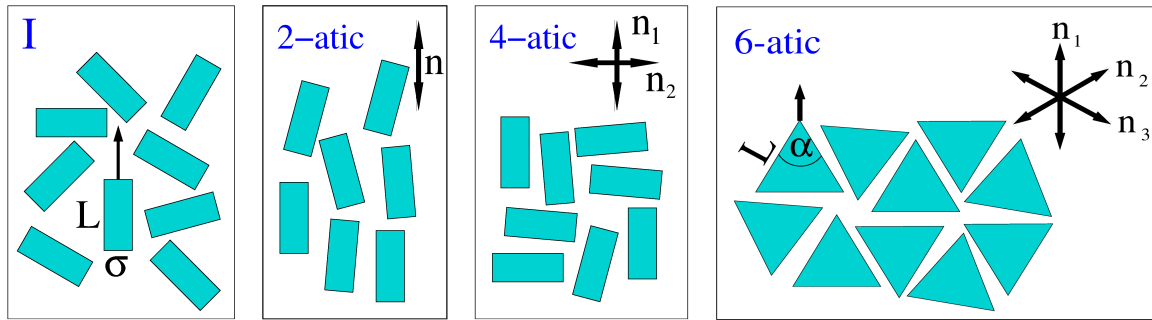


FIG. 2: Sketches of liquid-crystal phases of HR and HT. Particle axes are indicated, together with the nematic directors of each phase.

behavior of hard-body fluids. The 2D version of this theory for a general fluid mixture of convex particles proposes the following expression for the excess part of the free-energy density:

$$\Phi_{\text{ex}}[\{\rho_i\}] \equiv \frac{\beta \mathcal{F}_{\text{exc}}[\{\rho_i\}]}{A} = -\rho \log(1 - \eta) + \frac{\sum_{i,j} \langle \langle A_{ij}^{(\text{spt})}(\phi) \rangle \rangle}{1 - \eta}, \quad (1)$$

with  $\beta = (k_B T)^{-1}$  and  $A$  the total area of the system. In the above expression the packing fraction of the mixture,  $\eta$ , is defined as

$$\eta = \sum_i \rho_i a_i, \quad \rho_i = \int_0^{2\pi} d\phi \rho_i(\phi), \quad (2)$$

with  $\rho_i$  the number density of the  $i$ th species, while  $a_i$  is its particle area. The total number density is just  $\rho = \sum_i \rho_i$ . The functions  $A_{ij}^{(\text{spt})}(\phi)$  are defined in terms of the excluded area between particles of species  $i$  and  $j$ , with their axes forming a relative angle  $\phi$ :

$$A_{ij}^{(\text{spt})}(\phi) = \frac{1}{2} [A_{ij}^{(\text{excl})}(\phi) - a_i - a_j]. \quad (3)$$

The symbol  $\langle \langle \dots \rangle \rangle$  means the double angular average with respect to  $\rho_i(\phi)$  and  $\rho_j(\phi)$ :

$$\langle \langle A_{ij}^{(\text{spt})}(\phi) \rangle \rangle \equiv \int_0^{2\pi} d\phi_1 \int_0^{2\pi} d\phi_2 \rho_i(\phi_1) \rho_j(\phi_2) A_{ij}^{(\text{spt})}(\phi_1 - \phi_2). \quad (4)$$

It is easy to show that the expression (1) recovers the exact Onsager second-virial form in the low-density limit  $\rho_i \rightarrow 0$ . Also, more sophisticated versions of DFT, namely those based on the Fundamental Measure Theory, have SPT as their uniform density limit [38].

In Fig. 1 we plot two examples of SPT areas (scaled with particle area) between two hard squares and two hard equilateral triangles. In these cases particles are chosen as having equal shape and size (same species). We note the symmetry of these functions: for squares the excluded area has a  $\pi/2$ -symmetry,  $A_{11}^{(\text{spt})}(\phi) = A_{11}^{(\text{spt})}(\phi + \pi/2)$ , while for equilateral triangles a  $2\pi/3$ -symmetry,  $A_{22}^{(\text{spt})}(\phi) = A_{22}^{(\text{spt})}(\phi + 2\pi/3)$ , is apparent. These symmetries in turn imply that the only possible orientationally ordered phases for squares and triangles must have orientational invariance by angles of  $\pi/2$  and  $\pi/3$ , i.e.  $\rho_1(\phi) = \rho_1(\phi + \pi/2)$  and  $\rho_2(\phi) = \rho_2(\phi + \pi/3)$ , respectively. These are the so called 4-atic and 6-atic orientationally ordered phases. Note that the  $2\pi/3$ -symmetry of the excluded area of equilateral triangles, together with the absence of a polar phase (the nematic directors and their  $\pi$ -rotated counterparts are equivalent) implies the  $\pi/3$  symmetry of triangles. In Fig. 2 we show sketches of the I, 2-atic and 4-atic phases for one-component HR and the 6-atic phase of triangles, while their typical probability density orientational distribution functions are shown in Fig. 3. These functions are defined in terms of the density profile  $\rho(\phi)$  as  $h(\phi) \equiv \rho(\phi)/\rho$  (with  $\int_0^{2\pi} d\phi h(\phi) = 1$ ). Note the presence of one (2-atic), two (4-atic) and three (6-atic) peaks of the same height (in  $[0, \pi]$ ) of the function  $h(\phi)$ , which shows the two-fold (2-atic), fourfold (4-atic) and sixfold (6-atic) orientational liquid-crystal symmetries.

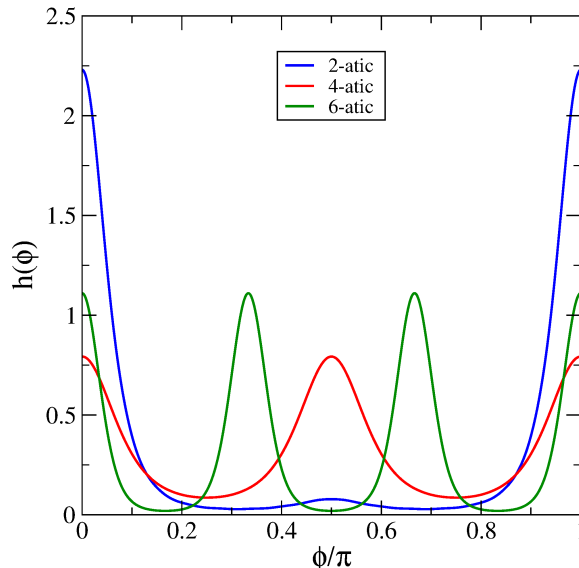


FIG. 3: The typical orientational distribution functions  $h(\phi)$  corresponding to 2-atic, 4-atic phases of HR, and 6-atic phase of HT.

The ideal part of the free-energy density is exact and has the expression

$$\Phi_{\text{id}}[\{\rho_i\}] \equiv \frac{\beta \mathcal{F}_{\text{id}}[\{\rho_i\}]}{A} = \sum_i \int_0^{2\pi} \rho_i(\phi) [\ln \rho_i(\phi) - 1], \quad (5)$$

where we have dropped the thermal areas.

The total free-energy density,  $\Phi[\{\rho_i\}] = \Phi_{\text{id}}[\{\rho_i\}] + \Phi_{\text{exc}}[\{\rho_i\}]$ , should be minimized with respect to  $\rho_i(\phi)$  to find the equilibrium configuration, for fixed values of the number densities  $\rho_i$ . The constrained minimization and the inversion of the minimized ideal part gives the following expression for  $\rho_i(\phi)$ :

$$\rho_i(\phi) = \frac{\rho_i e^{-c_i(\phi)}}{\int_0^{2\pi} d\phi' e^{-c_i(\phi')}}, \quad (6)$$

$$c_i(\phi) = \frac{\delta \Phi_{\text{exc}}[\{\rho_i\}]}{\delta \rho_i(\phi)} = -\ln(1 - \eta) + \tilde{c}_i(\phi) + \beta p a_i, \quad (7)$$

$$\tilde{c}_i(\phi) = \frac{2 \sum_j \int_0^{2\pi} d\phi' \rho_j(\phi') A_{ij}^{(\text{spt})}(\phi - \phi')}{1 - \eta}, \quad (8)$$

$$\beta p = \frac{\rho}{1 - \eta} + \frac{\sum_{i,j} \langle \langle A_{ij}^{(\text{spt})}(\phi) \rangle \rangle}{(1 - \eta)^2}, \quad (9)$$

As the terms  $-\ln(1 - \eta)$  and  $\beta p a_i$  (the scaled pressure) are the same in the exponentials of the numerator and denominator and do not depend on the angular coordinate, they cancel out, which results in

$$\rho_i(\phi) = \frac{\rho_i e^{-\tilde{c}_i(\phi)}}{\int_0^{2\pi} d\phi' e^{-\tilde{c}_i(\phi')}} \quad (10)$$

We now perform a bifurcation analysis to find the packing fraction value at which the I phase becomes unstable with respect to the 2-atic or 4-atic phases. It is useful to use a Fourier expansion of the density profiles:

$$\rho_i(\phi) = \rho_i h_i(\phi) = \frac{\rho_i}{2\pi} \left[ 1 + \sum_{k \geq 1} h_i^{(k)} \cos(2k\phi) \right], \quad (11)$$

with  $h_i(\phi)$  the orientational distribution function of species  $i$ , and  $h_i^{(k)}$  its  $k$ th Fourier amplitude. We define the Fourier coefficients of the SPT area as

$$A_{ij,k}^{(\text{spt})} \equiv \frac{1}{2\pi} \int_0^{2\pi} d\phi A_{ij}^{(\text{spt})}(\phi) \cos(2k\phi). \quad (12)$$

The analytic form of these coefficients can be found for hard-rectangle mixtures and hard-isosceles-triangle mixtures in Ref. [39] and [11], respectively. With these definitions, inserting Eqn. (11) into Eqn. (10), multiplying by  $\cos(2n\phi)$ , integrating from 0 to  $2\pi$ , and expanding the exponentials up to first order in the first Fourier amplitudes  $h_i^{(n)}$  (with  $n$  denoting the symmetry, and ( $n = 1$  for 2-atic,  $n = 2$  for 4-atic, and  $n = 3$  for 6-atic) we finally obtain a set of algebraic equations,

$$B \cdot \mathbf{h}^{(n)} = \mathbf{0}, \quad B_{ij} = \delta_{ij} + \frac{2A_{ij,n}^{(\text{spt})} \rho_j}{1 - \eta}, \quad (13)$$

with  $\mathbf{h}^{(n)}$  the column vector formed by the Fourier amplitudes  $\{h_i^{(n)}\}$  of all species from  $i = 1$  up to  $i = c$  (the total number of components). This set has a nontrivial solution only if  $\mathcal{B}(\eta) \equiv \det(B) = 0$ . The latter is just the condition to find the packing fraction at bifurcation. For example for a binary mixture we find

$$\mathcal{B}(\eta) = 1 + 2 \frac{\overline{\rho A_{ii,n}^{(\text{spt})}}}{1 - \eta} + \frac{4\rho_1\rho_2}{(1 - \eta)^2} \det(A_n^{(\text{spt})}), \quad (14)$$

where we have defined

$$\overline{A_{ii,n}^{(\text{spt})}} = \sum_i x_i A_{ii,n}^{(\text{spt})}, \quad \det(A_n^{(\text{spt})}) = A_{11,n}^{(\text{spt})} A_{22,n}^{(\text{spt})} - \left(A_{12,n}^{(\text{spt})}\right)^2, \quad (15)$$

with  $x_i = \rho_i/\rho$  the molar fraction of the  $i$ th species. Taking into account that, for the particle geometries we are considering in this work, we have  $\det(A_n^{(\text{spt})}) = 0$ , from the bifurcation condition  $\mathcal{B}(\eta) = 0$  we obtain the packing fraction at bifurcation as

$$\eta_n = \frac{1}{1 - 2\overline{A_{ii,n}^{(\text{spt})}}/\bar{a}_i}, \quad \bar{a}_i = \sum_i x_i a_i. \quad (16)$$

The degree of orientational ordering of species  $i$  in the mixture can be quantified through the order parameters  $Q_2^{(i)}$  (2-atic) and  $Q_4^{(i)}$  (4-atic) for HR, and also  $Q_8^{(i)}$  (8-atic) for HRT and  $Q_6^{(i)}$  (6-atic) for equilateral triangles. They are defined as

$$Q_{2n}^{(i)} = \int_0^{2\pi} d\phi h_i(\phi) \cos(2n\phi) = \frac{h_i^{(n)}}{2}. \quad (17)$$

In the case where a mixture exhibits a first-order transition, the two-phase coexistence curves are calculated through the equalities of the chemical potentials of the coexisting phases  $\alpha$  and  $\beta$  for each species, and the equality of pressure at  $\alpha$  and  $\beta$ , both of which guarantee chemical and mechanical equilibrium, i.e.

$$\mu_i(\{\rho_i^{(\alpha)}\}) = \mu_i(\{\rho_i^{(\beta)}\}), \quad p(\{\rho_i^{(\alpha)}\}) = p(\{\rho_i^{(\beta)}\}), \quad (18)$$

where the chemical potentials and pressure are calculated from  $\Phi[\{\rho_i\}]$  as

$$\beta\mu_i = \frac{\partial\Phi}{\partial\rho_i}, \quad \beta p = \sum_i \rho_i(\beta\mu_i) - \Phi. \quad (19)$$

The explicit expression for  $\beta p$  is given by Eqn. (9), while the chemical potential of species  $i$ ,  $\mu_i = \mu_i^{(\text{id})} + \mu_i^{(\text{exc})}$ , can be divided into ideal and excess part. The ideal part is

$$\beta\mu_i^{(\text{id})} = \ln \rho_i + \int_0^{2\pi} d\phi h_i(\phi) \ln h_i(\phi), \quad (20)$$

while the excess part can be computed as

$$\beta\mu_i^{(\text{exc})} = -\ln(1-\eta) + \frac{2\sum_j \rho_j \langle\langle A_{ij}^{(\text{spt})}(\phi)\rangle\rangle_{h_{i,j}}}{1-\eta} + \beta p a_i, \quad (21)$$

where

$$\langle\langle A_{ij}^{(\text{spt})}(\phi)\rangle\rangle_{h_{i,j}} \equiv \int_0^{2\pi} d\phi h_i(\phi) \int_0^{2\pi} d\phi' h_j(\phi') A_{ij}^{(\text{spt})}(\phi - \phi'). \quad (22)$$

For a one-component fluid all the above expressions are the same but sums over species and indexes are omitted. The extension of SPT to include not only the second,  $B_2[h]$ , but also the third,  $B_3[h]$ , virial coefficient for the one-component fluid can be implemented by replacing the expression (1) for the excess part of the free-energy density by

$$\Phi_{\text{exc}}[\rho] = \rho \left\{ -\ln(1-\eta) + \frac{\eta}{1-\eta} b_2[h] + \left( \frac{\eta}{1-\eta} + \log(1-\eta) \right) (b_3[h] - 2b_2[h]) \right\}, \quad (23)$$

where we have defined the scaled (with particle area  $a$ ) virial coefficients as

$$b_k[h] = \frac{B_k[h]}{a^{k-1}} - 1. \quad (24)$$

The coefficient  $b_2[h]$  is just the doubled angular average of the scaled function  $A^{(\text{spt})}(\phi)$  with respect to the orientational distribution function  $h(\phi)$ , i.e.  $b_2[h] = a^{-1} \langle\langle A^{(\text{spt})}(\phi)\rangle\rangle_h$ . The third virial coefficient is defined as

$$B_k[h] = \frac{1}{3} \prod_{i=1}^3 \left( \int_0^{2\pi} d\phi_i h(\phi_i) \right) \mathcal{K}^{(3)}(\phi_1, \phi_2, \phi_3), \quad (25)$$

$$\mathcal{K}^{(3)}(\phi_1, \phi_2, \phi_3) = -\frac{1}{A} \left( \prod_{i=1}^3 \int_A d\mathbf{r}_i \right) f(\mathbf{r}_{12}, \phi_{12}) f(\mathbf{r}_{23}, \phi_{23}) f(\mathbf{r}_{13}, \phi_{13}), \quad (26)$$

with  $f(\mathbf{r}_{ij}, \phi_{ij})$  the Mayer function of particle  $i$  and  $j$ , with relative spatial and angular variables  $\mathbf{r}_{ij} = \mathbf{r}_i - \mathbf{r}_j$  and  $\phi_{ij} = \phi_i - \phi_j$  respectively. For details of the bifurcation analysis using this extended theory see Refs. [10, 12].

### III. THEORETICAL RESULTS

This section presents the results obtained from the numerical implementation of the SPT for rectangular and triangular particles of one-component fluids. The case of a quaternary mixture of HRT is also discussed as a model for a fluid with strong clustering effects. We concentrate on the description of phase diagrams and bifurcations to orientationally ordered phases. Special attention is paid to the effect of clustering on the orientational properties of HRT.

#### A. One-component fluids

We define a 2D liquid-crystal model of particles consisting of monodisperse HR of length  $L$  and width  $\sigma$ , with aspect ratio  $\kappa = L/\sigma \geq 1$ . The SPT area between two rectangles with relative angle  $\phi$  between their main axes (the main axis being parallel to the long axis  $L$ ), which is the main ingredient of SPT, can be calculated as

$$A^{(\text{spt})}(\phi) = \frac{L^2 + \sigma^2}{2} |\sin \phi| + L\sigma |\cos \phi|. \quad (27)$$

As shown in Sec. II, this expression defines the theoretical model completely. Note that, since the fluid is monodisperse, subindices for the different species can be eliminated.

MC simulations of hard squares (HS) [14] and HR of aspect ratio  $\kappa = 2$  [15] showed the existence of a 4-atic stability window between the I and the crystalline phase. The latter, in the case of HR of  $\kappa = 2$ , also exhibits 4-atic ordering with square dimers at perpendicular orientations, tesseling the whole area at close packing. Recent simulations showed

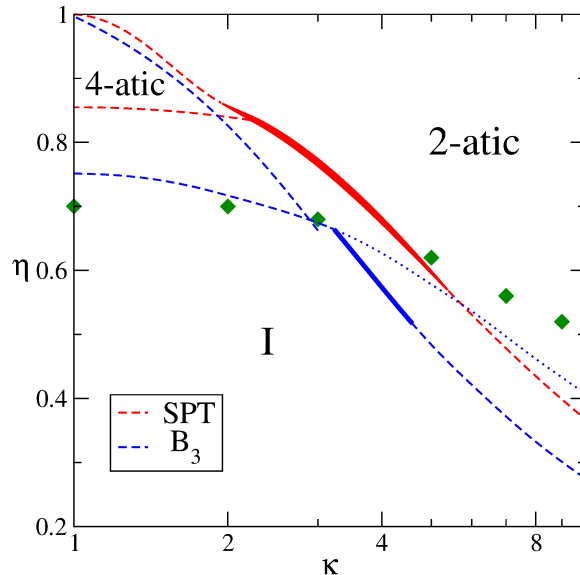


FIG. 4: Phase diagrams of HR in the  $\eta$ - $\kappa$  plane from the standard SPT approximation and the extension including  $B_3$  (as indicated in the legend). Solid and dashed lines indicate first- and second-order transitions, with filled regions corresponding to two-phase coexistence gaps. Labels correspond to regions of stability of I, 4-atic and 2-atic phases. The dotted line is the extension of the I-T bifurcation curves from the  $B_3$ -theory to the  $\kappa$  values where 4-atic is unstable with respect to the 2-atic phase. Our MC simulation results for the location of the I-T (for  $\kappa \lesssim 7$ ) or I-N transition are shown with filled rhombuses.

that the 4-atic phase is stable up to  $\kappa \sim 5$  [40], while experiments on monolayers of granular cylinders of aspect ratios as large as 7 showed the existence of stationary states exhibiting 4-atic textures [22, 26].

The first calculation of the I-4-atic and I-2-atic second-order transitions for a HR fluid was done in Ref. [8], which established the stability of the 4-atic phase for  $\kappa < 2.61$  [8]. However the two-phase coexistence lines and the 2-atic-4-atic second-order transition were not calculated. The numerical implementation of SPT for the HR fluid gives the phase diagram plotted in Fig. 4, in the packing fraction ( $\eta$ )-aspect ratio ( $\kappa$ ) plane [9]. We only accounted for uniform phases, but here the coexistence binodals and the 2-atic-4-atic spinodal line are also included. It can be seen that, at high  $\eta$ , SPT predicts a stable 4-atic phase after a second-order I-4-atic transition for  $\kappa \lesssim \kappa_{ce} \approx 2.21$ . This is the position of the critical-end point, where the I-4-atic bifurcation curve (calculated from Eqn. (16) with  $n = 2$ ) and the (I,4-atic)-binodal of the first order (I,4-atic)-2-atic transition coalesce. The 4-atic phase stability region is bounded above by a 2-atic-4-atic transition, which can be of first or second order, with the 2-atic-4-atic tricritical point located at  $\kappa_{t_1} \approx 1.94$ . For  $\kappa > \kappa_{ce}$ , the I phase exhibits a first-order transition to the 2-atic phase up to  $\kappa \leq \kappa_{t_2} \approx 5.44$ , the position of the I-2-atic tricritical point. Beyond this value of aspect ratio, the I-2-atic transition is always of second order and the bifurcation curve is given by Eqn. (16) with  $n = 1$ . The results from the  $B_3$  theory are also plotted in Fig. 4 [10]. The main differences with respect to the SPT are: (i) The I-4-atic bifurcation occurs at much lower packing fractions. (ii) The position of the critical end-point moves to higher values,  $\kappa_{ce} \approx 3.1$ . These two facts together cause the stability region of the 4-atic phase to be much wider. Also, the I-2-atic transition curve moves to lower packing fractions when three-body correlations are included. The onset of stability for the 4-atic phase compares favourably with our own MC simulations (rhombuses for  $\kappa \lesssim 7$ ). This result points to the relevance of three-body, and possibly higher-order, correlations to quantitatively predict the phase behavior of 2D fluids of hard anisotropic particles.

We now turn to triangular particles. A collection of isosceles triangles of equally sized edge-lengths  $L$  and opening angle  $\alpha$  define a one-component fluid of hard isosceles triangles. The SPT area between two particles with relative orientation  $\phi$  (the particle axis defined to be parallel to the bisector of the opening angle) can be calculated from

$$A^{(\text{spt})}(\phi) = L^2 \begin{cases} \sin \alpha \cos \phi, & 0 \leq \phi \leq \alpha, \\ \frac{1}{2} \sin(\alpha + \phi), & \alpha \leq \phi \leq (\pi - \alpha)/2, \\ \sin \phi - \frac{1}{2} \sin(\alpha + \phi), & (\pi - \alpha)/2 \leq \phi \leq \pi. \end{cases} \quad (28)$$



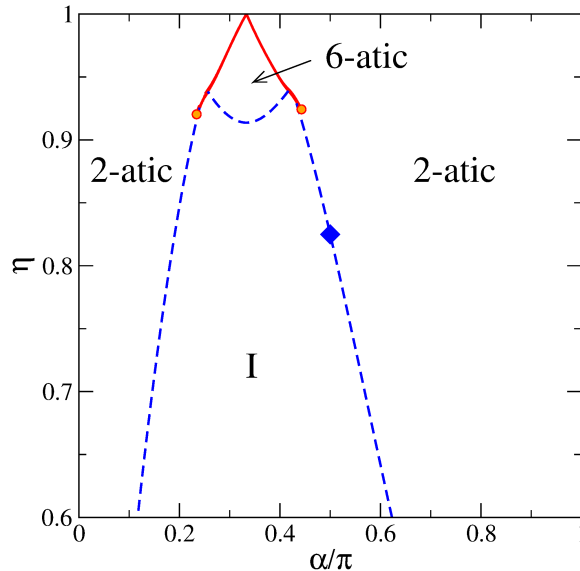


FIG. 5: Phase diagram of HT in the  $\eta$ - $\alpha$  plane from SPT. With dashed lines we show the second-order transition lines while the solid lines indicate first order transitions. The regions of stability of I and the orientationally ordered 2-atic and 6-atic phases are labeled. With solid circles we show I-2-atic critical points. The rhombus indicates the packing fraction value of the I-2-atic bifurcation of HRT ( $\alpha = \pi/2$ ).

for  $\alpha \leq \pi/3$ , while for  $\alpha \geq \pi/3$

$$A^{(\text{spt})}(\phi) = L^2 \begin{cases} \sin \alpha \cos \phi, & 0 \leq \phi \leq (\pi - \alpha)/2, \\ (1 - \cos \alpha) \sin \phi, & (\pi - \alpha)/2 \leq \phi \leq \alpha, \\ \sin \phi - \frac{1}{2} \sin(\alpha + \phi), & \alpha \leq \phi \leq \pi. \end{cases} \quad (29)$$

In SPT these expressions completely define the model and the thermodynamics of the fluid. The phase diagram in the packing fraction  $\eta$ -opening angle  $\alpha$  plane is plotted in Fig. 5. Equilateral triangles, due to their intrinsic sixfold symmetry (invariance with respect to  $\pi/3$ -rotation), can only form an orientationally ordered 6-atic phase (see Fig. 2). But isosceles triangles with opening angle  $\alpha \simeq \frac{\pi}{3}$  also stabilize this phase via a second order I-6-atic transition, shown as a dashed line in Fig. 5. The 6-atic phase is bounded above by a first-order 6-atic-2-atic transition, which ends in two critical points (filled circles). As the opening angle is increased up to  $\pi$ , or decreased down to 0, obtuse or acute triangles turn into hard needles. It is clear that if the aspect ratio of the particles, defined through the opening angle as  $\kappa = \cot(\alpha/2)$ , increases or decreases, the fluid exhibits a second order I-2-atic at high enough packing fractions (dashed line of Fig. 5 separating the regions of I and 2-atic phase stability). Although it is reasonable to expect that particles with  $\kappa \ll 1$  or  $\kappa \gg 1$  (close to the Onsager limit) will stabilize the 2-atic phase, the situation is not clear for isosceles triangles with opening angle around  $\pi/2$ , i.e. hard right triangles (HRT), whose location in the phase diagram of Fig. 5 is shown by a rhombus.

Recent simulations [12, 20] showed that a fluid of HRT stabilizes a 4-atic phase, with the presence of 8-atic correlations, and that the orientational distribution function,  $h(\phi)$ , has a total of eight peaks in the interval  $[0, 2\pi]$ . If all the peaks had exactly the same height the global phase would be 8-atic. As can be seen from the figure, there is no indication of 4-atic or 8-atic phase stability for  $\alpha \sim \pi/2$ . Motivated by the fact that this result could be a defect of the SPT (a second-virial theory), we have implemented the I to  $p$ -atic bifurcation analysis (with  $p = 2, 4, 6$  and 8), using the  $B_3$  theory, with an excess free-energy density given by Eqn. (23) [12]. The results are shown in Table I. Clearly the lowest value of packing fraction corresponds to the I-2-atic bifurcation. A free-energy minimization for values of  $\eta$  above this bifurcation confirms the 2-atic phase stability, with the equilibrium distribution function showing the usual peaks at 0 and  $\pi$  (see Fig. 3) and the absence of any satellite peaks. The reason why the DFT with two or three-body correlations incorporated cannot predict the 4-atic or 8-atic phase stability will be explained in Sec. III B.

Bifurcation	I-2-atic	I-4-atic	I-6-atic	I-8-atic
$\eta_n$ from SPT	0.8249	0.9928	0.9821	0.9444
$\eta_n$ from $B_3$ -theory	0.7325	0.9794	0.9328	0.8353

TABLE I: Values of the packing fractions  $\eta_n$  at I-2-atic ( $n = 1$ ), I-4-atic ( $n = 2$ ), I-6-atic ( $n = 3$ ) and I-8-atic ( $n = 4$ ) bifurcations from the SPT and the  $B_3$ -theory.

### B. Clustering effects in fluids of triangles modeled as a quaternary mixture

To explore the symmetry and stability of fluids made of HRT particles, we have performed NVT and NPT MC simulations of systems of 576 particles [12]. Different compression and expansion protocols were performed. Fig. 6 shows the 4-atic and 8-atic order parameters  $Q_4$  and  $Q_8$  as a function of packing fraction  $\eta$ . Clearly, compression of the fluid from the I phase brings about an increase in the  $Q_8$  order parameter, while the 4-atic order parameter  $Q_4$  stays at a low value. This points to strong 8-atic correlations in the fluid, with an orientational distribution function (not shown) having eight peaks of similar height in the interval  $[0, 2\pi]$ . When compression is continued up to high packing fractions, the system remains in the 8-atic phase. Expanding a previously prepared 4-atic crystal (with a square unit cell made of four self-assembled triangles forming a tetramer) from very high packing fractions, a stable crystal is obtained down to the melting point, where a 4-atic liquid-crystal phase is formed with high values of  $Q_4$  and  $Q_8$  vanishing small (the nature of this phase transition cannot be ascertained from our results). This 4-atic phase remains stable up to  $\eta \sim 0.72$ , below which  $Q_4$  abruptly drops to zero. This behavior of  $Q_{2n}$  shows that the system exhibits strong hysteresis in the region where the 8-atic and 4-atic phases are present, an indication that the I-4-atic transition is strongly of first order. The MC free-energy calculations of the 4-atic and crystalline phases carried out by the authors of Ref. [20] indicate that the 4-atic phase is the stable liquid-crystal phase. In Fig. 6 label B indicates the two-phase coexistence region obtained from Ref. [20], while regions C and D correspond to the regions of stability of the 4-atic and crystal phases, respectively [20].

We have also prepared a crystalline phase with a unit cell now made of square dimers obtained by joining two triangles by their hypotenuses, and the hypotenuses of all triangles being parallel to each other along the crystal. This is a perfect crystal with  $Q_2 = 1$ . After expanding this crystal, it eventually melts to a 2-atic liquid-crystal phase with a high value of  $Q_2$  [12]. The system continues to be metastable up to values of  $\eta$  when  $Q_2$  drops to zero. This behavior implies that, although the 2-atic phase is metastable, the free-energy difference between the 2-atic and 4-atic phases should be small.

From the preceding discussion we can conclude that the fluid of HRT exhibits strong 8-atic correlations by expanding the I phase from low densities, but the 4-atic is the stable liquid-crystal phase. As pointed out in Sec. II both, the SPT and the  $B_3$ -theory (the latter including two and three-body correlations), predict that the I phase bifurcates to a 2-atic phase, which remains stable above the bifurcation. Thus the DFT fails to correctly predict the symmetry of the stable liquid-crystal phase. This failure is related to the fact that the standard DFT formalism, based on the one-body density, cannot take into account the effect of clustering or self-assembling of particles. If we try to assemble a 4-atic or 8-atic (apart from I and 2-atic) phase made of HRT by resorting to configurations with strong particle clustering, something similar to the configuration sketched in Fig. 7 results. Note how a 4-atic phase can be obtained by the presence of a large amount of square tetramers, formed by self-assembling of four triangles (the monomer units) joined by their short edge-sides. The diagonals of these square tetramers are oriented on average along two mutual perpendicular and equivalent directions. The 8-atic phase could be obtained by the presence of these tetramers, but a large amount of square dimers formed by two triangles joined by their hypotenuses have to be added. If these hypotenuses are oriented along the same directions of the tetramer orientations, the fluid will exhibit strong 8-atic correlations, i.e. the orientational distribution function will have eight sharp peaks in the interval  $[0, 2\pi]$ .

A very simplified model to account for particle clustering is to treat the one-component fluid of HRT as a quaternary mixture, with species defined as following (see Fig. 8): (i) The first species is of square geometry and made by a dimer formed by joining two triangular monomer units by their hypotenuses. This species will have a molar fraction  $x_1^{(1)}$  (we adopt the convention of using the subindex to label the geometry: 1 for the square and 2 for the triangle, and the superindex to label the size: 1 for small and 2 for large size), and has  $L_1^{(1)} = L$  as the square side length and  $a_1^{(1)} = L^2$  as particle area (see Table II). (ii) The second species again is square but defined by a tetrameral cluster, i.e. four triangles joined by their short sides, with a molar fraction  $x_1^{(2)}$ , side length  $L_1^{(2)} = \sqrt{2}L$  and area  $a_1^{(2)} = 2L^2$ . (iii) The third species is a triangular monomer unit of side length  $L_2^{(1)} = L$  and area  $a_2^{(1)} = L^2/2$ , with the molar fraction labelled as  $x_2^{(1)}$ . And (iv) the last species is a triangular dimer formed by two monomer units joined by their short sides, with the right angles of the triangles being in contact (see Fig. 8); the equally sized

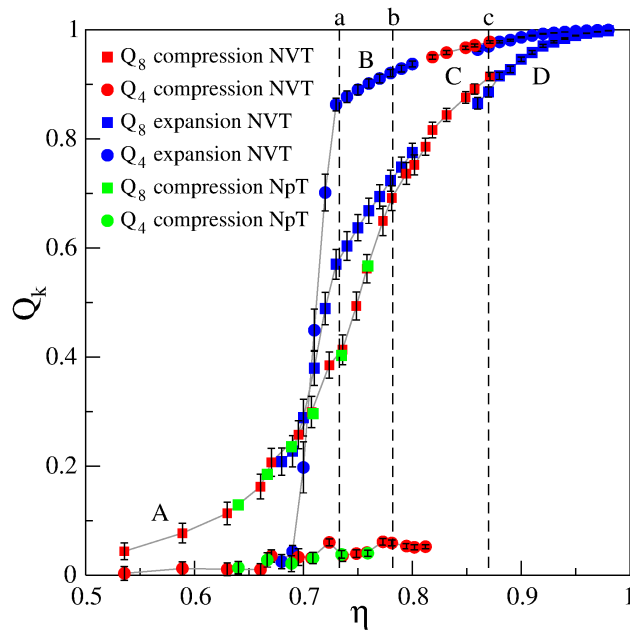


FIG. 6: Order parameters  $Q_4$  and  $Q_8$  vs. packing fraction  $\eta$  obtained from NVT and NPT MC simulations of a fluid of HRT. Different expansion and compression protocols were taken, as indicated. Label A indicates the region of stability of the I phase, label B the I–4-atic phase coexistence region, and labels C and D indicate the region of stability of 4-atic and crystal phases, respectively, as they were obtained in Ref. [20].

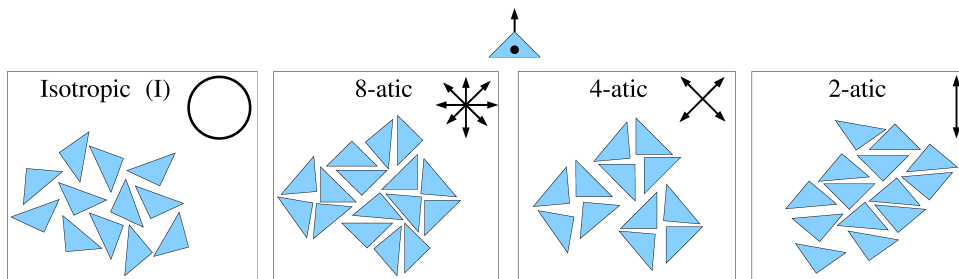


FIG. 7: Sketches of I, 8-atic, 4-atic and 2-atic phases of a HRT fluid, where strong clustering of triangles can induce the corresponding liquid-crystal symmetries. Also shown are the equivalent directors of these phases, having twofold (2-atic), fourfold (4-atic) and eightfold (8-atic) symmetries.

side lengths are  $L_2^{(2)} = \sqrt{2}L$ , the area  $a_2^{(2)} = L^2$ , and the molar fraction  $x_2^{(2)}$ . Obviously these triangular species are needed in our model because two of them, with the adequate relative orientation, will form a tetramer. See Table II for a summary of the parameters. Note that there are more possible dimers: one formed by selecting one of the two possible configurations resulting (i) by sticking two triangular units by their short sides, but with the right and acute angles of the triangles in contact, and (ii) the other from a specular reflection of the latter with respect to the axis passing through the triangular heights (see Fig. 8). We discarded these dimers with rhomboidal shape for the sake of simplicity but, as shown later, they certainly appear in MC simulations.

We used the SPT described in Sec. II to numerically minimize the total free-energy with respect to the orientational distribution functions of all four species  $\{h_i^{(j)}(\phi)\}$ . The aim was to look for the existence of a set of molar fractions  $\{x_i^{(j)}\}$  for which the resulting distribution function of monomers  $h_m(\phi)$  has 8-atic symmetry. The sum over species is taken over the subindexes and superindexes of all quantities involved in the SPT. For example the SPT area now reads  $A_{ij}^{(\text{spt},kl)}(\phi)$ , and depends on the set of the characteristic side lengths of species  $\{L_i^{(j)}\}$ , and the sum over species of the double angular average should be substituted by  $\sum_{i,j,k,l=1,2} \langle \langle A_{ij}^{(\text{spt},kl)}(\phi) \rangle \rangle$ . The total packing fraction of the

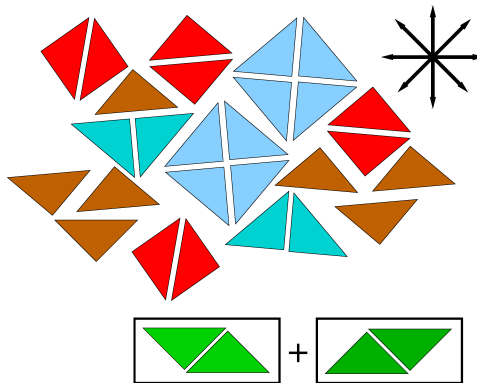


FIG. 8: Sketches of the four types of clusters used in the theoretical model, represented in different colors. The rhomboidal clusters discarded in our model are shown at the bottom.

mixture is now defined as  $\eta = \sum_{i,j=1,2} \rho_i^{(j)} a_i^{(j)}$  with  $\rho_i^{(j)} = x_i^{(j)} \rho$  the number density of species  $ij$ .

From  $\{h_i^{(j)}(\phi)\}$  we can calculate the monomer distribution function  $h_m(\phi)$ , i.e. the probability density of triangular monomer units being oriented with respect to a fixed laboratory axis with angle  $\phi$ . The expression that relates these magnitudes can be found in Ref. [41]. From  $h_m(\phi)$  we can calculate the order parameters as  $Q_{2n}^{(m)} = \int_0^\pi d\phi h_m(\phi) \cos(2n\phi)$ . In Fig. 9 (a) we show all the distribution functions  $\{h_i^{(j)}(\phi)\}$  for the following fixed values of molar fractions:  $x_1^{(1)} = 0.4$ ,  $x_1^{(2)} = 0.15$ ,  $x_2^{(1)} = 0.35$  and  $x_2^{(2)} = 0.1$ . The scaled pressure was fixed to  $\beta pa_2^{(1)} = 220$ . As we can see, these distribution functions correspond to a 4-atic phase, with all distribution functions fulfilling the fourfold symmetry  $h_i^{(j)}(\phi) = h_i^{(j)}(\phi + \pi/2)$ . This phase is the equilibrium phase, due to the presence of a large amount of square clusters, whose fourfold symmetry dictates the symmetry of the phase. Interestingly, triangular monomers and dimers follow the same 4-atic symmetry of square clusters. However their distribution functions exhibit the presence of two more satellite peaks of lower height at  $\phi = \pi/4$  and  $\phi = 3\pi/4$ . Although  $h_2^{(1,2)}(\phi)$  does not fulfill the 8-atic symmetry (invariance with respect to rotations by  $\pi/4$ ), triangular clusters certainly exhibit some 8-atic correlations, which is directly related to the crossed excluded area between squares and triangles (the expression can be found in Ref. [41]). This function has local minima at relative angles of  $\pi/4$  and  $3\pi/4$ . But the most remarkable result is the symmetry of the angular distribution function of monomers  $h_m(\phi)$  resulting from the  $\{h_i^{(j)}(\phi)\}$  functions; this is shown in Fig. 9 (b). We can see the quasi-8-atic symmetry,  $h_m(\phi) \sim h_m(\phi + \pi/4)$ , of monomers. This result proves that strong clustering of particles into superparticles of square and triangular symmetries can induce 8-atic ordering, the one observed in MC simulations by compressing the I fluid. In panel (c) the order parameters of monomers  $Q_{2n}^{(m)}$  are plotted as a function of the monomer molar fraction  $x_2^{(1)}$  for the same fixed pressure and along the following path of molar fractions:  $x_1^{(1)} = x_2^{(1)} + 0.05$ ,  $x_1^{(2)} = 0.5 - x_2^{(1)}$ ,  $x_2^{(2)} = 0.45 - x_2^{(1)}$  with  $x_2^{(1)}$  varying in the interval  $[0, 0.45]$ . There is an interval about  $x_2^{(1)} \approx 0.33$  where the order parameter  $Q_8$  is the highest one as compared to  $Q_2$  and  $Q_4$ . This indicates the presence of strong 8-atic correlations. Strong 8-atic correlations are also obtained for other selected paths (not shown here), and it can be concluded that, for some cluster compositions, a quasi-8-atic symmetry can be easily obtained. Of course this model is oversimplified in the sense that the molar fractions are fixed. An extended SPT theory, supplemented by chemical equilibrium conditions between different clusters and monomers at fixed packing fraction of monomers, together with the addition of rhomboidal clusters, would allow to find the equilibrium values of  $x_i^{(j)}$  and also explore the effect of rhomboidal clusters on the symmetry of liquid-crystal 4-atic and 8-atic phases.

Fig. 10 shows the results of a clustering analysis from equilibrated MC simulations of HRT at different packing fractions. Details of this analysis can be found in Ref. [41]. Two important features are apparent. when the I fluid is compressed (filled symbols) all clusters, except the monomer units, are more or less equally represented: see the packing-fraction region between 0.7 and 0.82 inside the liquid-crystal stability region. The compression run from the I fluid gave rise to 8-atic correlations. However, expansion runs from the 4-atic crystal (open symbols) at high packing fraction show strong clusterisation, with an excess of tetramers and the subsequent appearance of triangular and square dimers (but no rhomboidal dimers) which exhibit maxima as the packing fraction decreases and the crystal melts to the 4-atic liquid-crystal phase. Both set of branches (from low and high densities) approximately connect to each other.

As shown in this section, the standard DFT is very successful in explaining the symmetry of the equilibrium phases

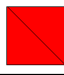
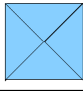


Species ( $ij$ )	11	12	21	22
Geometry				
$L_i^{(j)}$	$L$	$\sqrt{2}L$	$L$	$\sqrt{2}L$
$a_i^{(j)}$	$L^2$	$2L^2$	$L^2/2$	$L^2$

TABLE II: Summary of the geometries of all four species that define the clustering model. Also shown are the values of side lengths  $L_i^{(j)}$  and particle areas  $a_i^{(j)}$  of the different species.

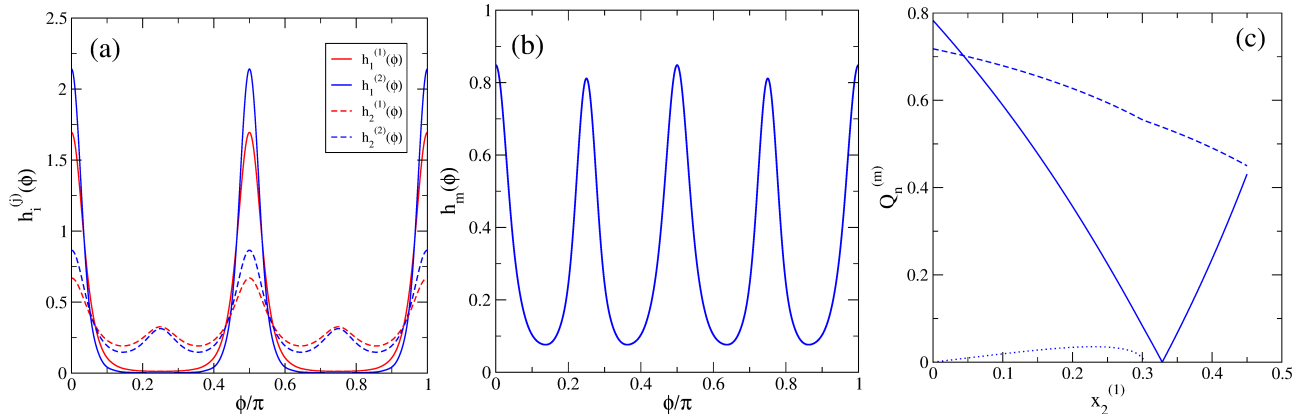


FIG. 9: (a) Orientational distribution functions of all four species for the set of molar fractions  $x_1^{(1)} = 0.4$ ,  $x_1^{(2)} = 0.15$ ,  $x_2^{(1)} = 0.35$ , and  $x_2^{(2)} = 0.1$ . Scaled pressure is fixed to  $\beta p a_2^{(1)} = 220$ . (b) The resulting monomer distribution function  $h_m(\phi)$ . (c) Order parameters  $Q_2$  (dotted),  $Q_4$  (solid) and  $Q_8$  (dashed) as a function of the molar fraction of monomers  $x_2^{(1)}$  with the constraint  $x_1^{(1)} = x_2^{(1)} + 0.05$ ,  $x_1^{(2)} = 0.5 - x_2^{(1)}$ ,  $x_2^{(2)} = 0.45 - x_2^{(1)}$ . Note that these constraints are such that  $x_1^{(1)} + x_2^{(2)} = x_1^{(2)} + x_2^{(1)}$ .

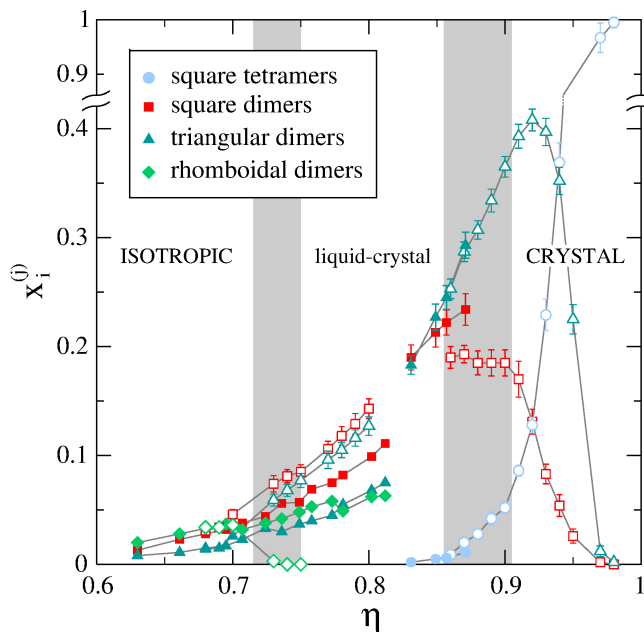


FIG. 10: Cluster compositions  $x_i^{(j)}$  as a function of  $\eta$  as obtained from MC simulations using compression (filled symbols) and expansion (open symbols) runs. See Ref. [41] for details. The regions of stability of the different phases are correspondingly labelled.

in the case of fluids made of hard rectangles and also of HT. However, in the case of HR, the extension of the theory to include the third virial coefficient points to the importance of high-order correlations and clustering. These effects are not enough to modify the symmetry of the bulk phases. But the HRT fluid is an example where these effects may be crucial, to the extent that the stable bulk phases may have a symmetry which does not follow from the particle shape, or from the symmetry of the excluded area between two particles.

#### IV. EXPERIMENTS ON VIBRATED GRANULAR PARTICLES

Vibrated monolayers of granular particles may be a valid approach to explore the symmetries of hard particles in 2D and the effects of entropy on the orientational properties of these fluids. In this sense they could play a role complementary to theory and simulation. Pioneering work by Narayan et al. [22] on vertically vibrated monolayers of anisotropic particles showed that granular particles such as rice, metallic cylinders or metallic pinwheels, can organise into liquid-crystalline 2D configurations. These configurations exhibit qualitatively similar properties as their thermal counterparts. For instance, in the steady-state regime, well-defined values of various order parameters can be obtained. Galanis et al. [23, 24] have also shown that some aspects of ordering in granular rods, when confined into cavities, can be explained in terms of the standard elastic free energy of nematics in competition with a surface energy. Since these early works, some effort has been devoted to map the phase diagram of cylinders [26, 27], which project as quasi-rectangles, as a function of packing fraction, based on the values of 2-atic and 4-atic order parameters. These studies showed that phase boundaries between isotropic, 2-atic 4-atic regions reasonably coincide with those derived from equilibrium DFT calculations. More recently, we have shown [27, 28] that geometrical frustration induced by circular boundaries gives rise to the excitation of topological defects in monolayers of cylindrical particles, which seem to obey the same rules, based on topological charge conservation, as in equilibrium systems governed by a continuous tensor order parameter. These similarities are very remarkable, given the essentially different physics that operates

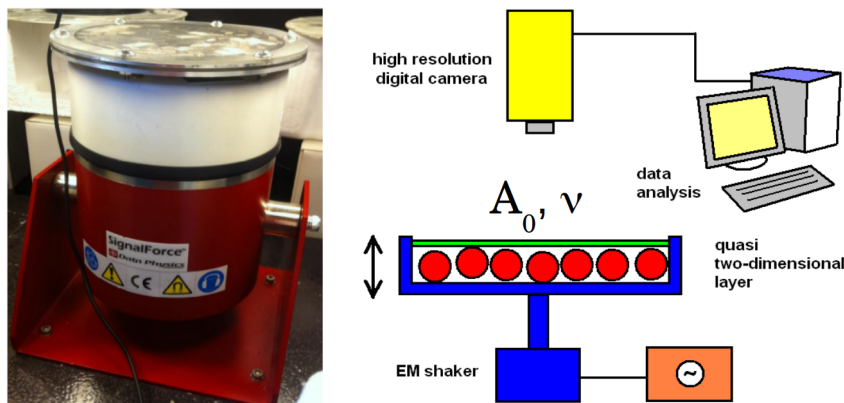


FIG. 11: Schematic of the experimental setup.

in systems of granular particles as opposed to systems in thermal equilibrium. It seems that collections of dissipative particles in highly-packed arrangements, subject to the continuous injection of energy via agitation, may reach steady-state configurations that can be understood in terms of entropic arguments, with a minimal contribution from nonequilibrium effects, which can be largely suppressed if experimental parameters are chosen adequately (these effects can be quantified as a slightly larger tendency of particles to form long-lived local arrangements [27]). Therefore, as shown in Section II, entropy alone can explain the existence of orientational ordering in high-density fluid monolayers of granular rods under vibration.

Fig. 11 is a schematic of the experimental setup. Steel particles 1.2 mm in width and an aspect ratio of 4 are confined into a circular cavity 16 cm in diameter and 2 mm in height. The system is quasi-2D since particles cannot pass over each other. The set is vibrated in the vertical direction with a frequency  $\nu$  close to 100 Hz, and an amplitude  $A_0$  which is adjusted so that the average acceleration  $\Gamma = A_0\nu^2/g$  is in the range 2-3, where  $g$  is the acceleration of gravity. With these settings, and at the packing-fraction regimes investigated, the local particle density is quite uniform and no large fluctuations can be detected. Spontaneous global rotation of the whole sample is sometimes excited but the analysis of the results subtract this mode. As an example, consider Fig. 12, which shows the local 4-atic order parameter  $Q_4$  in a monolayer with packing fraction  $\eta \simeq 0.7$ . The local ordering field can be defined in

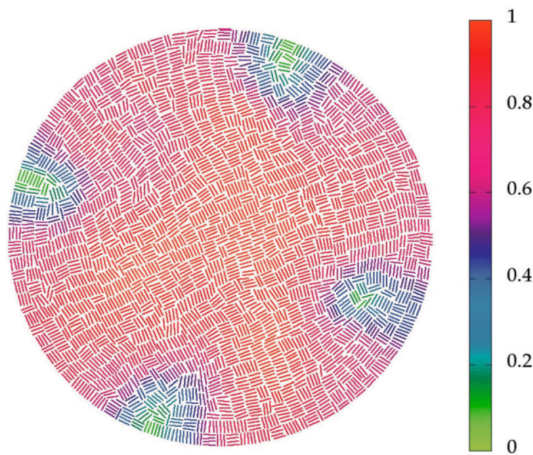


FIG. 12: Colour map of the  $Q_4$  order parameter of a granular monolayer of cylinders of aspect ratio 4 at packing fraction  $\eta = 0.70$ . A global 4-atic symmetry is apparent, but with four point defects which are clearly visible at regions with a depleted order parameter.

terms of order parameters, based on Eqn. (17) but calculated locally over particles inside a small circular region. The local nematic director is calculated by diagonalising the local order tensor, and all the order parameters  $Q_{2n}$  can be obtained from this reference direction. In this configuration a high value of  $Q_4$  can be seen throughout most of the system (on the contrary, the value of  $Q_2$ , not shown, is very low).

As mentioned above, the similarities between dissipative and equilibrium systems are not based simply on the observation that order parameters can be defined and that orientational ordering appears more or less abruptly as density is increased. An ordering local field can also be defined in the system. When subject to conflicting boundaries with symmetries different from the inherent symmetries of the configurations, point defects, where the orientational field can no longer be defined, are excited. Fig. 12 shows a typical example where a globally 4-atic configuration of confined rectangles (projected steel cylinders) exhibits four point defects located close to the cavity wall, forming a square. This is the expected configuration of repelling defects, and leads to the conclusion that there is an elastic field through which defects interact at long distances. An elastic analogy may help elucidate the nature of these point defects. The Frank elastic free energy is

$$F_{\text{el}} = \frac{1}{2} \int_A d\mathbf{r} \left[ K_1 (\nabla \cdot \hat{\mathbf{n}})^2 + K_3 |\hat{\mathbf{n}} \times (\nabla \times \hat{\mathbf{n}})|^2 \right], \quad (30)$$

where  $\hat{\mathbf{n}}$  is the nematic field (director), and  $K_1, K_3$  the elastic moduli associated to splay and bend, respectively. In 2D nematics the twist mode is obviously absent. Note that in a 4-atic phase the two equivalent directors are orthogonal,  $\hat{\mathbf{n}} \perp \hat{\mathbf{m}}$ , so that the splay mode of one corresponds to the bend mode of the other, and Eqn. (30) is closed with respect to all possible modes. This results, based on symmetry grounds, implies that  $K_1 = K_3 \equiv K$ , so that the elastic free energy can be written as

$$F_{\text{el}} = \frac{1}{2} K \int_A d\mathbf{r} |\nabla \theta|^2, \quad (31)$$

where  $\mathbf{n} = (\cos \theta, \sin \theta)$ , and  $\theta$  is the local orientation of the director. This is the free energy of the  $xy$  model, which is known to contain vortices as elementary excitations. Thus, the equilibrium configuration of  $\theta(\mathbf{r})$  obeys Laplace's equation (harmonic solutions). The elementary excitation of this model, spin waves and local vortices or topological defects, can be created spontaneously through thermal fluctuations, but defects can be driven by geometrical constraints. This is the case in our granular monolayers.

The nature of the defects can be obtained by examining the elastic field in the neighbourhood of the defects. These are described in terms of a phase  $\theta_0$  and a winding number  $k$ . Far from the defect the harmonic field is  $\theta(\mathbf{r}) = \theta_0 + k\varphi$ , where  $\mathbf{r} = r(\cos \varphi, \sin \varphi)$ . According to topology theory, there is a relation between the p-rotational symmetry of the phase and the winding number, given by the topological charge  $q$  of the defect:

$$q = \frac{2\pi w}{2\pi/p} = wp \quad (32)$$



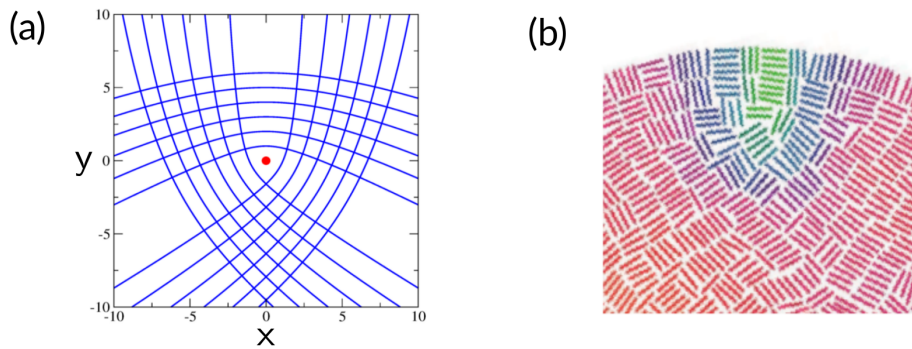


FIG. 13: (a) Director field in the neighbourhood of a point defect with winding number  $w = +1/4$ . (b) Particle configurations in the region surrounding a point defect. Colour indicates the value of  $Q_4$ . A closed loop surrounding the defect has been drawn. The triangular symmetry of this loop (with curved sides) clearly matches the one resulting from the elastic field in panel (a), which indicates that the defect in the granular monolayer corresponds to a winding number  $w = +1/4$ .

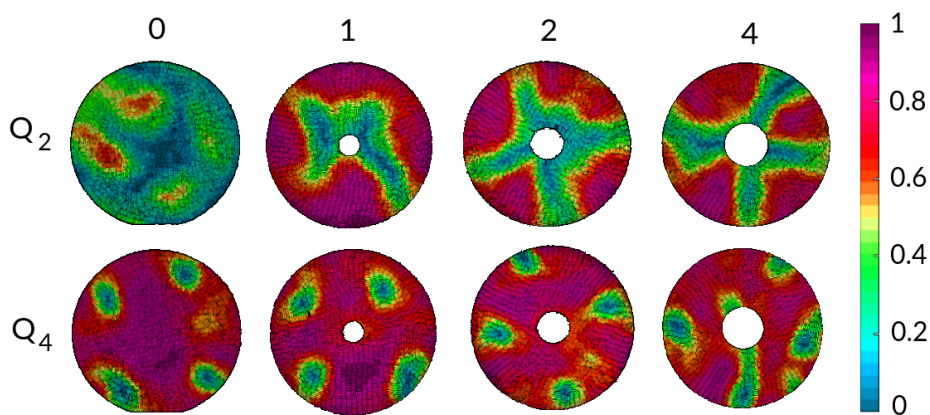


FIG. 14: Colour maps of order parameters  $Q_{2n}$ , with  $n = 1, 2$  and  $4$ . Columns are labelled by the numbers  $0, 1, 2, 4$ , which correspond to the size (in cm) of the central obstacle in the cavity.

In addition, Euler's theorem implies that there is a conservation of the total topological charge,

$$q_t = \sum_i q_i = p\chi, \quad (33)$$

where the sum extends over all defects in the system and  $\chi$  is the Euler characteristics of the container. For a disc (circular cavity) or a square,  $\chi = 1$ ; for an annulus,  $\chi = 0$ , and so on.

Fig. 13 (a) shows a solution for the elastic field, in the neighbourhood of a singularity of the field, using a winding number  $w = +1/4$ , corresponding to a charge  $q = 1$  ( $p = 4$  for the tetratic). In panel (b) a real configuration of the particles in a defected region is shown. The local orientation of the particles has been sketched. Clearly the overall symmetry of both fields, theoretical and experimental, coincide, which leads one to conclude that the circular cavity is actually generating defects with topological charge  $+1$ . In view of Eqn. (33), it is immediately clear that topology predicts four  $+1$  defects in the circular cavity, and this is indeed the case. Note that other possibilities, with other types of defects of different charge, could also exist in general; in this case four  $+1$  point defects are the only valid solution, as observed in the experiment. We have looked at a more complicated cavity, the annulus. Here, two concentric circular walls confine the particles, one with positive curvature and the other with negative curvature. Particles confined in this type of containers have been examined before [42]. However, we must keep in mind that topology predictions rely on the continuum approximation. In our case this means that particle size should be much less than any typical scale in the container. In the case of the circular cavity, the ratio  $R/l$ , where  $R$  is the cavity



radius and  $l$  the length of the particle, is  $\sim 20$ . For the annulus we should focus on the inner wall,  $R_{\text{in}}$ . In Fig. 14 we show maps of the different order parameters for different values of  $R_{\text{in}}$ : 5, 10 and 20 mm. This implies values  $R_{\text{in}}/l = 1.25, 2.5$  and 5, which may be too small for the continuum approximation to be valid. The predictions of topology theory may thus be compromised. We will see that this is actually the case.

For an annulus  $\chi = 0$ , and Eqn. (33) predicts a total topological charge of 0. This does not mean necessarily that there are no defects in the system, but that the *total* charge should be zero. Therefore, it is obvious that a solution for the elastic field with only distortion, and no defects, is a possibility. This is presumably the solution with the lowest free energy. However, this is not what happens. Instead, a complex pattern is excited. The pattern consists of smectic regions, characterised by a high value of  $Q_2$ , separated by regions of 4-atic order containing a point defect. Up to four smectic regions can be seen in Fig. 14. The two types of regions are separated by domain walls. The system without obstruction (left column) does not exhibit these structures. In small nematic samples subject to distortion domain walls can be excited (see e.g. [43]). These structures are not contemplated by the simple elastic theory supplemented by point defect, but might result by extending elastic theory to incorporate domain walls, or  $D - 1$ -dimensional defects, where  $D$  is the dimension of physical space. Anyway the continuum limit may be broken down in this case and more detailed analysis would be required to explain the complex structures shown in Fig. 14.

Many other confining geometries and particle shapes can be explored with the present setting. For example, it would be interesting to explore particles with triangular shape, which may present different types of inherent order. As shown by our theoretical DFT calculations, equilateral triangles stabilise a p-atic phase with  $p = 6$ . A configuration with six  $q = +1$  defects is expected in a cavity with  $\chi = 1$ . But there may be differences as regards not only how these defects appear in the cavity, but also the number and values of the defect charges, as the only requirement involves the total charge in the cavity. Another interesting system will be a fluid of right-angles triangles. As discussed in Section II, clustering effects may give rise to strong 8-atic correlations in the fluid through the formation of relatively stable compact arrangements of particles which generate orientational order along complementary directions and bulk phases with secondary directors. Whether this feature may or may not affect the number of nature of the defects remains to be seen. Also, since clustering is expected to be stronger in the granular system than in a similar system in thermal equilibrium, the cluster distribution and the fractions of different types of clusters may change substantially in experimental granular monolayers subject to vibration.

## V. CONCLUSION

In this work we have summarised the current status of our own investigations on the ordering properties and liquid-crystalline phases of 2D hard particles of polygonal shapes. Our approach is based on the interplay between two views: an equilibrium view, obtained by using our standard DFT functional based on the SPT approximation and extensions, together with computer simulations, and a nonequilibrium view, based on experiments on vibrated monolayers of quasi-two dimensional particles. These two systems, although very different from a physical point of view, seem to meet at some point in terms of ordering behaviour and response to external fields. Experiments can be used to verify the predictions of the theory, while the theory can suggest new experiments which can be useful to test these predictions.

In general, DFT predictions are qualitatively correct, in that the symmetry of the phases and the overall region of stability with respect to density and particle sizes are reasonably predicted, with the agreement even improving when three-body correlations are included. However, we have examined a case where DFT fails dramatically: the case of right-angled triangles. In this system simulations indicate a strong tendency for the system to develop 4-atic and 8-atic correlations, due to the strong tendency of particles to locally arrange in dimers (of square, triangular and rhomboidal shapes) and tetramers (of square shape). As a result, the symmetry of the bulk phase may be different from the one dictated by the geometry of the particles. It then seems that clustering may be very important for some nonregular polygonal shapes, giving rise to nontrivial symmetries than cannot be predicted by the standard DFT theories based on two-, or even three-body correlations.

Based on the above findings, two future lines of research can be identified. On the one hand, improved DFT theories, incorporating particle clustering in a consistent way (not as imposed static clusters with predefined fractions as in Section III B), may be worthwhile to develop. In parallel, and view of the success of experiments based on vibrated monolayers, new granular particles can be explored in different geometries, in an effort to extract information on the symmetries of the system by looking at local order parameters and at the elementary localised excitations that result when that inherent symmetries are subject to geometric frustration through confinement by different types of cavities.

## Acknowledgments

Financial support from Grant No. PGC2018-096606-B-I00 (MCIU/AEI/FEDER,UE) is acknowledged.

- 
- [1] K. Zhao, C. Harrison, D. Huse, W. B. Russel, and P. M. Chaikin, *Phys. Rev. E* **76**, 040401R (2007).
  - [2] K. Zhao, R. Bruinsma, and T. G. Mason, *Nat. Commun.* **3**, 801 (2012).
  - [3] K. Zhao, R. Bruinsma, and T. G. Mason, *PNAS* **108**, 2684 (2011).
  - [4] S. C. Glotzer and M. J. Solomon, *Nat. Mater.* **6**, 557 (2007).
  - [5] P. F. Damasceno, M. Engeland, and S. C. Glotzer, *Science* **337**, 453 (2012).
  - [6] D. Wang, M. Hermes, S. Najmr, N. Tasios, A. Grau-Carbonell, Y. Liu, S. Bals, M. Dijkstra, C. B. Murray, and A. van Blaaderen, *Nat. Commun.* **13**, 6001 (2022).
  - [7] D. de las Heras, Y. Martínez-Ratón, L. Mederos, and E. Velasco, *J. Mol. Liq.* **185**, 13 (2013).
  - [8] H. Schlacken, H.-J. Mogel, and P. Schiller, *Mol. Phys.* **93**, 777 (1998).
  - [9] Y. Martínez-Ratón, E. Velasco, and L. Mederos, *J. Chem. Phys.* **122**, 064903 (2005).
  - [10] Y. Martínez-Ratón, E. Velasco, and L. Mederos, *J. Chem. Phys.* **125**, 014501 (2006).
  - [11] Y. Martínez-Ratón, A. Díaz-De Armas, and E. Velasco, *Phys. Rev. E* **97**, 052703 (2018).
  - [12] Y. Martínez-Ratón and E. Velasco, *Phys. Rev. E* **104**, 054132 (2021).
  - [13] M. A. Bates and D. Frenkel, *J. Chem. Phys.* **112**, 10034 (2000).
  - [14] K. W. Wojciechowski and D. Frenkel, *Comput. Methods Sci. Technol.* **10**, 235 (2004).
  - [15] A. Donev, J. Burton, F. H. Stillinger, and S. Torquato, *Phys. Rev. B* **73**, 054109 (2006).
  - [16] A. Buhot and W. Krauth, *Phys. Rev. E* **59**, 2939 (1999).
  - [17] C. Avendaño and F. A. Escobedo, *Soft Matter* **8**, 4675 (2012).
  - [18] J. A. Anderson, J. Antonaglia, J. A. Millan, M. Engel, and S. C. Glotzer, *Phys. Rev. X* **7**, 021001 (2017).
  - [19] D. A. Tripllett and K. A. Fitchhorn, *Phys. Review E* **77**, 011707 (2008).
  - [20] A. P. Gantapara, W. Qi, and M. Dijkstra, *Soft Matter* **11**, 8684 (2015).
  - [21] A. H. Lewis, I. Garlea, J. Alvarado, O. J. Dammone, P. D. Howell, A. Majumdar, B. M. Mulder, M. P. Lettinga, G. H. Koenderink, and D. G. A. L. Aarts, *Soft Matter* **10**, 7865 (2014).
  - [22] V. Narayan, N. Menon, and S. Ramaswamy, *J. Stat. Mech.* (2006) P01005.
  - [23] J. Galanis, D. Harries, D. L. Sackett, W. Losert, and R. Nossal, *Phys. Rev. Lett.* **96**, 028002 (2006).
  - [24] J. Galanis, R. Nossal, W. Losert, and D. Harries, *Phys. Rev. Lett.* **105**, 168001 (2010).
  - [25] I. C. Garlea, O. Dammone, J. Alvarado, V. Notenboom, Y. Jia, G. H. Koenderink, D. G. A. L. Aarts, M. P. Lettinga, and B. M. Mulder, *Sci. Rep.* **9**, 20391 (2019).
  - [26] T. Müller, D. de las Heras, I. Rehberg, and K. Huang, *Phys. Rev. E* **91**, 062207 (2015).
  - [27] M. González-Pinto, F. Borondo, Y. Martínez-Ratón, and E. Velasco, *Soft Matter* **13**, 2571 (2017).
  - [28] M. González-Pinto, J. Renner, D. de las Heras, Y. Martínez-Ratón, and E. Velasco, *New. J. Phys.* **21**, 033002 (2019).
  - [29] E. S. Harper, G. van Anders, and S. C. Glotzer, *PNAS* **116**, 16703 (2019).
  - [30] T. Vo and S. C. Glotzer, *PNAS* **119**, e2116414119 (2022).
  - [31] L. Onsager, *Ann. N. Y. Acad. Sci.* **51**, 627 (1949).
  - [32] H. Reiss, H. L. Frisch, and J. L. Lebowitz, *J. Chem. Phys.* **31**, 369 (1959).
  - [33] M. A. Cotter and D. E. Martire, *J. Chem. Phys.* **52**, 1902 (1970).
  - [34] M. A. Cotter and D. E. Martire, **53**, 4500 (1970).
  - [35] M. A. Cotter and D. C. Wacker, *Phys. Rev. A* **18**, 2669 (1978).
  - [36] G. Lasher, *J. Chem. Phys.* **53**, 4141 (1970).
  - [37] B. Barboy and W. Gelbart, *J. Chem. Phys.* **71**, 3053 (1979).
  - [38] P. Tarazona, J. A. Cuesta, and Y. Martínez-Ratón, *Lect. Notes Phys.* **753**, 247 (2008).
  - [39] Y. Martínez-Ratón, E. Velasco, and L. Mederos, *Phys. Rev. E* **72**, 031703 (2005).
  - [40] I. Torres-Díaz, R. S. Hendely, A. Mishra, A. J. Yeh, and M. A. Bevan, *Soft Matter* **18**, 1319 (2022).
  - [41] Y. Martínez-Ratón and E. Velasco, *Phys. Fluids* **34**, 037110 (2022).
  - [42] I. C. Garlea, P. Mulder, J. Alvarado, O. Dammone, D. G. A. L. Aarts, M. P. Lettinga, G. H. Koenderink, and B. M. Mulder, *Nature Communications* **7**, 12112 (2016).
  - [43] D. de las Heras and E. Velasco, *Soft Matter* **10**, 1758 (2014).